Energetics of plastic bending of carbon nanotubes

Hideki Mori,[1] Shigenobu Ogata,[2,3,4] Ju Li,[5] Seiji Akita,[1] and Yoshikazu Nakayama[1,4,*]
[1]*Department of Physics and Electronics, Osaka Prefecture University, 1-1 Gakuen-cho, Sakai, Osaka 599-8531, Japan*
[2]*Center for Atomic and Molecular Technologies, Osaka University, Osaka 565-0871, Japan*
[3]*Department of Mechanical Engineering, Osaka University, Osaka 565-0871, Japan*
[4]*Handai Frontier Research Center, Osaka University, Osaka 565-0871, Japan*
[5]*Department of Materials Science and Engineering, Ohio State University, Columbus, Ohio 43210, USA*
(Received 27 May 2006; revised manuscript received 4 August 2006; published 25 October 2006)

Plastic bending of single-wall carbon nanotubes is analyzed using minimum energy path calculation with a bond-order potential. The calculation demonstrates that plastic deformation is only thermodynamically favorable above a threshold "yield curvature" ρ_{yield}, and is kinetically feasible above 1500 K, which agree with our experimental observations. A deformation mechanism map as function of temperature and bending curvature is constructed, and the dependence of ρ_{yield} on the nanotube diameter is analyzed.

DOI: 10.1103/PhysRevB.74.165418 PACS number(s): 81.07.De, 62.20.Fe, 62.25.+g, 81.05.Zx

I. INTRODUCTION

Like the shape forming of macroscopic objects, controlled plastic deformation of carbon nanotube (CNT) is vital for its adoption in nanoscale electronic and mechanical devices. Recently, Nakayama *et al.* succeeded in *in-situ* observation of the plastic deformation of carbon nanotubes in transmission electron microscope (TEM).[1] They used Pt-coated scanning probe microscope (SPM) tip to induce bending, and simultaneously passed electrical current through the CNT. The tube is resistively heated to a temperature exceeding 1000 K, and upon withdrawal of both the current and the bending force, the tube is found to be plastically bent. This does not occur if there is no current (resistive heating), in which case the tube bends and unbends elastically.

Like bulk crystals, nanotubes are thought to deform by the nucleation and motion of dislocations. In an originally perfect nanotube, the dislocations must be nucleated in pairs, the smallest embryo of which is the so-called 5-7-7-5 (Stone-Wales) defect.[2] It can be formed by 90° rotation of a single bond in the graphene plane, which transforms four adjacent hexagons into two pentagons and two heptagons. This 5-7-7-5 defect can then dissociate into a 5-7 defect (+ dislocation) and a 7-5 defect (– dislocation), by successive 90° rotation of neighboring C-C bonds.[3] Although the role of the 5-7-7-5 defect nucleation[4–12] and the 5-7 defect migration[3,6] in the plastic deformation[13–16] of nanotubes has been identified theoretically for many years, it is only recently that the 5-7 defects have been directly observed in high-resolution TEM.[17] A crucial difference between one-dimensional (1D) nanotubes and three-dimensional (3D) bulk crystals is the lack of the Frank-Read source,[18] since dislocations in nanotubes are not line defects, so the usual ways of dislocation multiplication (by for instance double cross-slip) are denied to the nanotubes. Therefore in contrast to bulk materials, nucleation may be a problem in their plastic deformation.[3,5,6]

This paper investigates defect nucleation and migration pathways involved in plastic bending, building upon previous theoretical work.[3–12,19–21] We analyze SWNTs using minimum energy path (MEP) calculation[22,23] and a bond-order potential.[24] The time at temperature and mechanical conditions to accomplish plastic bending are predicted. The model shows that plastic bending is only thermodynamically favorable above a threshold "yield curvature"ρ_{yield}, and is kinetically feasible above 1500 K, which agree with our experimental observations.[1] A deformation mechanism map is constructed at the end as a function of temperature and bending curvature.

II. PLASTIC BENDING MODEL AND NUMERICAL METHOD

Two single-wall carbon nanotube (SWNT) are examined: (5,5) armchair type and (8,0) zigzag type, which have nearly equal diameter of 0.66 nm. The tube length of both models is ~6.3 nm. The number of atoms is 520 and 480 for the (5,5) and (8,0) models, respectively. To limit our search of the potential energy landscape, we make the following assumptions about the plastic deformation. First, the nanotubes keep sp^2 bond network in all processes. Second, processes generating a square or an octagon are not allowed. Third, atoms are not inserted or removed. In the initial, elastically bent state, we refer to position of the maximum tensile stress as the "back position," and position of the maximum compressive stress as the "belly position" [see Fig. 1(a)]. Generally speaking, 5-7-7-5 defect nucleation and the migration of split 5-7 pairs will produce local strain fields on top of the imposed strain, and will also cause chirality changes.[3,19–21]

In armchair type SWNT, the 5-7-7-5 defect is nucleated at the back position, and splits into two 5-7 pairs, which attract each other if without the imposed strain. With the imposed bending strain, the pairs glide away towards the belly position, changing the chirality from (n,n) to $(n,n-1)$ in the domain between the two defects. On the other hand, in zigzag type SWNT, the 5-7-7-5 defect is nucleated at the belly position, and splits into two 5-7 pairs, which are driven by the bending strain to glide towards the back position, changing the chirality from $(n,0)$ to $(n,1)$ in the domain in between. For example, the armchair type changes its chirality from (5,5) to (5,4) at the back position, and the zigzag type changes its chirality from (8,0) to (8,1) at the belly position. This relaxes the local tensile and compressive strain, respec-

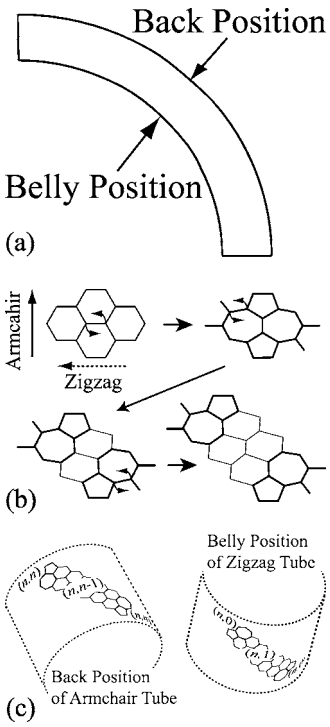

FIG. 1. (a) The back and belly positions of bent SWNT, (b) plastic deformation accomplished by bond rotation (adapted from Ref. 3), (c) first nucleation event in armchair SWNT and zigzag SWNT, respectively.

tively [see Figs. 1(b) and 1(c)]. Nucleation of the 5-7-7-5 defect at the other site in each model is energetically less favorable. In the (5,5) tube, while the formation energy of nucleating the 5-7-7-5 defect decreases from 3.1 eV to −1.9 eV with increasing tensile strain from 0.0 to 0.1, it only decreases from 3.1 eV to 0.7 eV with increasing compressive strain of the same magnitude. On the other hand, in the (8,0) tube, while the formation energy of nucleating the 5-7-7-5 defect decreases from 3.0 eV to −1.2 eV with increasing compressive strain, it only decreases from 3.0 eV to 0.4 eV with increasing tensile strain. This justifies first nucleation event under tension at the back position in (5,5) tube, and under compression at the belly position in (8,0) tube.

We use the nudged elastic band (NEB) method,[25] an efficient technique for finding the MEP between specified initial and final states,[22,23] to investigate the energetics of 5-7-7-5 defect nucleation, dissociation, and 5-7 defect migration. In NEB calculation, a chain of "connected images" interpolating the initial and final states is allowed to relax towards the MEP that goes through the saddle point of the transformation. For interatomic potential, we use the analytic bond-order potential for carbon, which produces accurate binding energies for graphite and diamond.[24,26,27] This potential is derived for the σ and π bonds of *sp*-valent systems by approximating the many-atom expansion for the bond order within the two-center, orthogonal tight-binding scheme.

In our NEB calculations, force acting on each atom is relaxed to less than 0.05 eV/Å, using simulated annealing relaxation. The activation and formation energies of 5-7-7-5 defect in the (5,5) straight SWNT (stress-free) are estimated to be 8.0 and 3.1 eV, respectively. They fit within range of recent theoretical studies based on density functional theory, 8.6–9.1 eV for the activation energy,[4,9,10] and 2.0–4.0 eV for the formation energy.[4–9]

III. RESULTS AND DISCUSSIONS

The activation and formation energies of 5-7-7-5 defect and the migration path of 5-7 pairs at finite bending curvature ρ are then calculated under fixed-displacement boundary condition at both ends of the tube. We show the MEP of nucleation of 5-7-7-5 defect and migration of 5-7 pairs at each bending condition in Figs. 2(a)–2(f). There are 11 "connected images" between the defect-free state (ND) and the state with the 5-7-7-5 defect (SW) and between each split step. The locally maximal energies in between each step denote the activation energies for transition. On the other hand, the locally minimal energies on each step denotes the formation energies of each step in reference to nondefective tube.

For straight and stress-free tubes [Figs. 2(a) and 2(d)], the formation energy increases with increasing split step. Obviously, 5-7-7-5 defect nucleation and pair migrations are thermodynamically unfavorable when there is no external stress. In bent tubes [Figs. 2(b), 2(c), 2(e), and 2(f)], the formation energies decrease with increasing split step. Figure 2 clearly shows the SWNTs prefer defective condition under large bending. In (5,5) type, when the 5-7 pairs glide four times, the configuration becomes energetically the most stable. In (8,0) type, when the 5-7 pairs glide six times, the configuration becomes the most stable. These globally optimal 5-7 pair positions are close to the neutral plane of the bent tube. With increasing bending curvature ρ, the activation energy for 5-7-7-5 defect nucleation decreases from 8.0 eV to 6.0 eV in (5,5) type and from 7.5 eV to 3.6 eV in (8,0) type. The activation energies for pair migration are not strongly dependent on ρ. They are 5.0 to 3.0 eV; average is 4 eV.

Since the highest barrier to plastic deformation in the experimental[1] range of ρ is the activation barrier for 5-7-7-5 defect nucleation, as shown in Figs. 2(b), 2(c), 2(e), and 2(f), we plot it as a function of bending curvature in Figs. 3(a) and 3(b). At bending curvature $\rho=0.34$ nm^{-1} for (5,5) type and 0.39 nm^{-1} for (8,0) type, we observed buckling instability. Therefore athermal nucleation, i.e., zero activation energy condition[28] for the 5-7-7-5 defect nucleation, does *not* occur before the buckling instability. The plastic deformation of unbuckled nanotubes therefore cannot take place without thermal activation. Quantitatively, the frequency of successful bond rotation depend on the temperature as $\nu \exp(-E_{\mathrm{act}}/k_{\mathrm{B}}T)$, where E_{act} is the activation barrier for 5-7-7-5 defect nucleation, and ν is the attempt frequency. Take $T=1500$ K, $\nu=10^{13}$ s^{-1}, and $E_{\mathrm{act}}=4.0$ eV. The frequency can be estimated to be 0.36 s^{-1}; thus, one bond rotation occurs every few seconds at $T=1500$ K. This temperature is lower than the estimated sublimation temperature of SWNT, 2500 K.[29] The result is consistent with our experimental observations,[1] the plastic deformation indeed occurs within a few seconds, at a current density that corresponds approximately to $T=1500$ K. For the (5,5) type tube, E_{act}

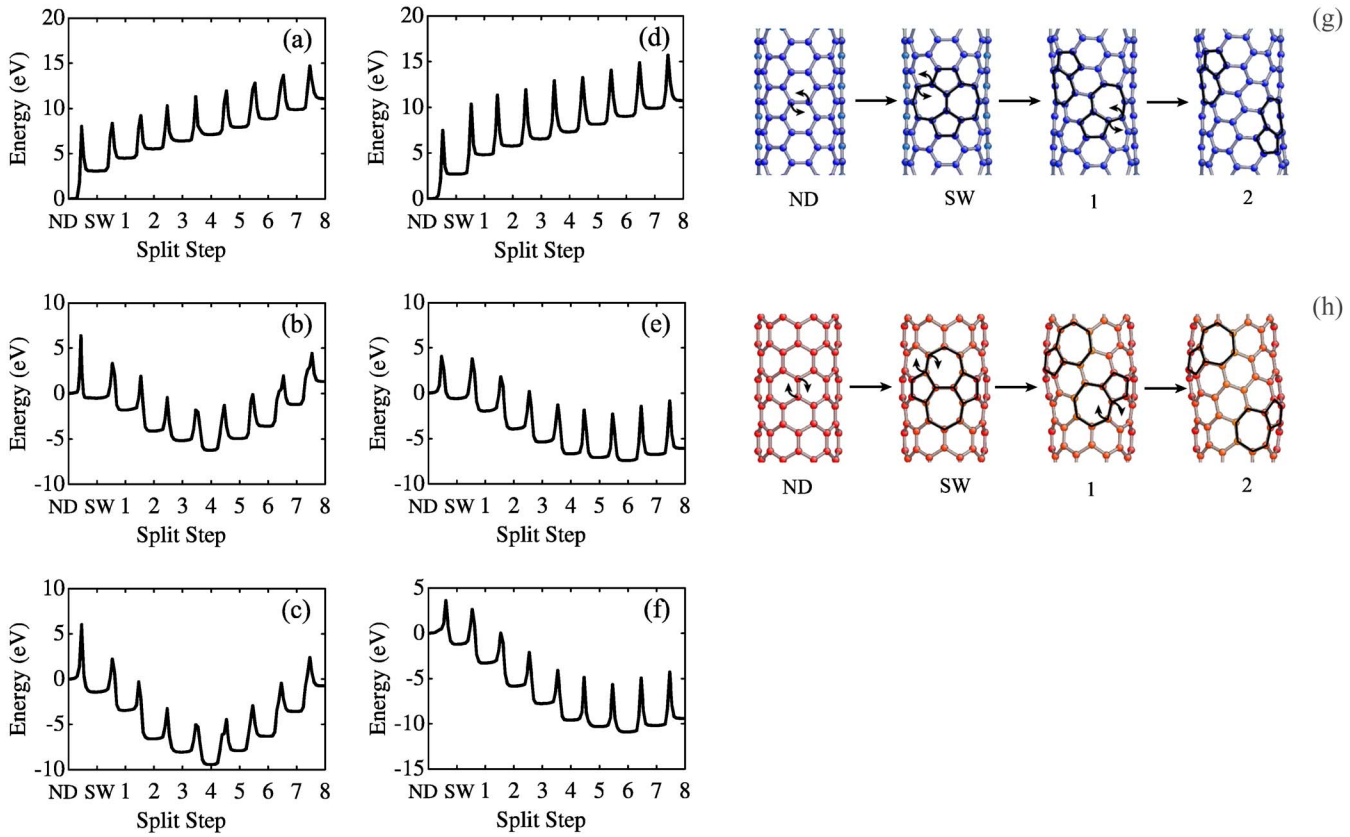

FIG. 2. (Color online) MEP of 5-7-7-5 defect nucleation and 5-7 pairs migration in (5,5) SWNT (a), (b), (c) and (8,0) SWNT (d), (e), (f) at bending curvature ρ=0 nm^{-1} (a), (d); 0.25 nm^{-1} (b), (e); and 0.34 nm^{-1} (c), (f). Labels "ND" and "SW" mean the defect-free state and the state with the 5-7-7-5 defect, respectively. x axis is the split step of the two pairs. Snapshots in (g) and (h) are the atomic configurations of each split step starting from (a) and (d), respectively.

=6.0 eV, a higher temperature is needed for 5-7-7-5 defect nucleation. However it is still lower than the sublimation temperature.

To identify the threshold for plastic deformation, i.e., "yield condition" in bending, we plot the formation energies of the optimally defective configurations in (5,5) and (8,0) nanotubes as a function of bending curvature, in Figs. 3(c) and 3(d). The 4 and 6 split-step configurations have the minimum potential energy over a wide range of ρ. The formation energy (in reference to nondefective tube) becomes negative at ρ_{yield}=0.11 nm^{-1} and 0.13 nm^{-1} for (5,5) and (8,0) SWNT, respectively. These results indicate that the plastically bent state becomes energetically more favorable than the elastically bent state above a "yield curvature" ρ_{yield}.

The significance of ρ_{yield} is that when bent below this curvature, the SWNT is *guaranteed* to deform elastically without any plastic deformation. This threshold behavior is the consequence of an interesting plastic confinement effect at the nanoscale, as illustrated in Fig. 4. The exact derivation is rather cumbersome, but an approximate scaling can be found straightforwardly. Roughly speaking, the 5-7 defects will migrate from the point of the highest stress to the neutral plane where the stress is zero. The stress decreases monotonically over an arc length L which is proportional to D, so the work done is approximately

$$W \approx b \int_0^L \sigma(L) dL = \lambda b \rho D^2, \tag{1}$$

where b is the Burgers vector, λ (unit N/m) is proportional to the Young's modulus of the graphene sheet, σ (unit N/m) is tensile stress. On the other hand, the energy it takes to nucleate a dislocation dipole and separate the two dislocations by L on a flat graphene sheet is

$$E(L) = 2E_{\text{core}} + A\lambda b^2 \ln(L/r_0), \tag{2}$$

where A is a dimensionless constant and E_{core} is the dislocation core energy.[30] Since the nanotube is graphene sheet wrapped around, the actual elastic interaction is not $\ln(L/r_0)$ but some other function $f(L \propto D) = g(D)$. The total energy trade-off is therefore approximately

$$E_f \equiv E - W \approx 2E_{\text{core}} + A\lambda b^2 g(D) - \lambda b \rho D^2, \tag{3}$$

which reaches critical balance E_f=0 at

$$\rho_{\text{yield}} \approx \frac{2E_{\text{core}}/\lambda b + Abg(D)}{D^2}. \tag{4}$$

The behavior of $f(L)$ is actually already plotted in Figs. 2(a) and 2(d), and we see that it can be reasonably approximated by a straight line in the range of L or D we are interested in.

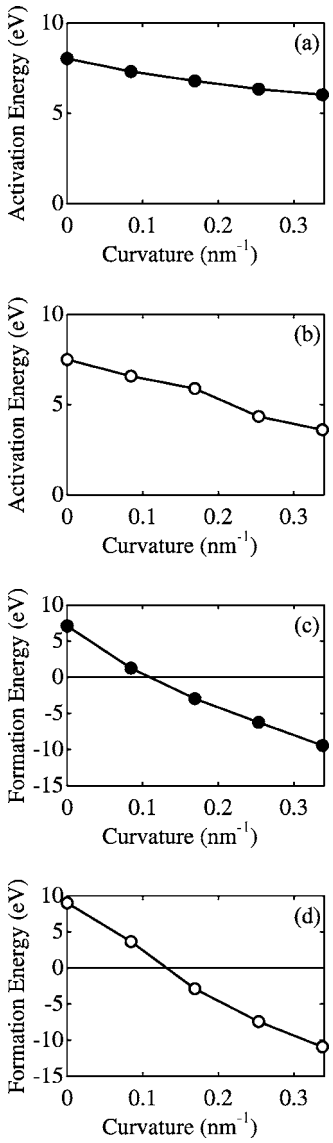

FIG. 3. Activation energies of 5-7-7-5 defect nucleation as a function of the bending curvature ρ, in (a) (5,5) SWNT, (b) (8,0) SWNT, and formation energies of the defective configuration of 4 and 6 split steps in (c) (5,5) SWNT, and (d) (8,0) SWNT, respectively, as a function of ρ.

This then means that ρ_{yield} should be roughly proportional to D^{-1}. We also see that for a fixed ρ, E_f should be a quadratic polynomial in D which is concave down. The actual results for the yield curvature ρ_{yield} are shown in Fig. 5(a), while the formation energies E_f for fixed $\rho=0.05$ nm^{-1} are shown in

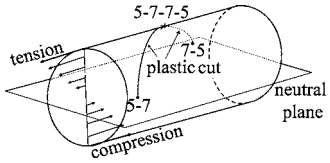

FIG. 4. Illustration of the total-energy model for the preference of plastic versus elastic deformation. The elastic energy can be relieved by 5-7-7-5 defect nucleation and 5-7 pairs migration (plastic cut), if that energy relief exceeds the self-energy of the plastic cut.

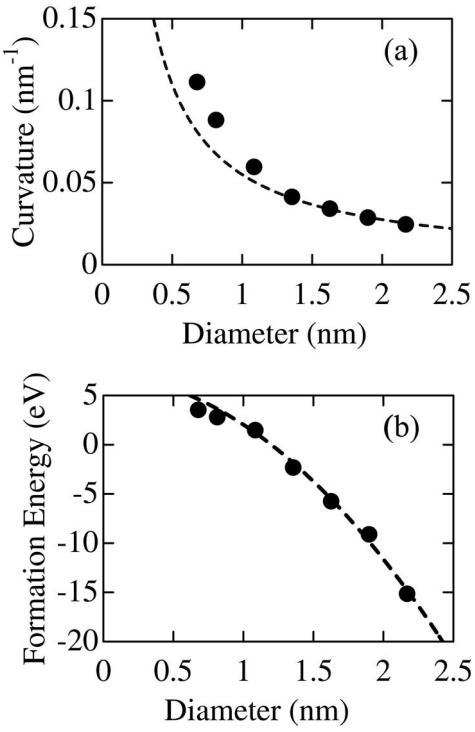

FIG. 5. (a) The yield curvature ρ_{yield} versus the tube diameter D. (b) The formation energies versus D at $\rho=0.05$ nm^{-1}. The dashed line in (a) and (b) is the approximate scaling (D^{-1} and $a_0+a_1D-a_2D^2$, respectively). The solid symbols are the actual numerical results.

Fig. 5(b). We see that the approximate scaling agrees quite well with the actual numerical results.

IV. DEFORMATION MECHANISM MAP

Our work is summarized in a deformation mechanism map, Fig. 6. For curvature $0<\rho<\rho_{\text{yield}}$, a nondefective tube bends elastically without any possibility of plastic deformation. For instance, we have obtained $\rho_{\text{yield}}=0.11$ nm^{-1} for (5,5) SWNT and 0.13 nm^{-1} for (8,0) SWNT from our calculations. Above ρ_{yield}, there is a large range of bending curvatures [$0.11<\rho<0.34$ nm^{-1} for (5,5) and $0.13<\rho<0.39$ nm^{-1} for (8,0)] where the SWNT can plastically deform, but only with appreciable rate if $T>1500$ K. The main rate-limiting step here is the first bond rotation that produces

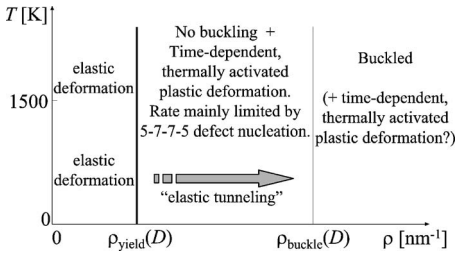

FIG. 6. Deformation mechanism map for bending SWNTs. Horizontal axis is the imposed curvature. Vertical axis is the temperature.

the 5-7-7-5 defect. Once plastic deformation has been accomplished at high temperatures, upon cooling and release of the bending force, the SWNT will still retain its bent form, allowing it to be shaped, which is vital for building nanoscale devices. The bent SWNT can only recover back to the straight form if it is heated to above 1500 K again, allowing the 5-7 defects to annihilate ("anneal"). At very large bending curvature, elastic buckling instability occurs. Preliminary calculations show that at $T=0$ K, the buckled SWNT do not nucleate defects spontaneously over yet another large range of bending, $\rho > \rho_{\text{buckle}}(D)$. Therefore, athermal plastic deformation[28] still does not happen immediately. However, time-dependent thermally activated plastic deformation is likely to happen on the buckled SWNT, and its rate is likely to be higher compared to the unbuckled SWNT due to the large local curvature. This regime is outside the scope of the present paper.

Many experimental conditions also take the "elastic tunneling" route shown in Fig. 6, especially at $T<800$ K. At these lower temperatures, the plastic deformation probability (within an experimental time scale of seconds) is so low that most specimen can escape through the plastic deformation regime all the way to the buckled regime without actually plastically deforming.

ACKNOWLEDGMENTS

The authors acknowledge support by the Ministry of Education, Science, Sports and Culture, Grant-in-Aid for Scientific Research on Priority Areas, Grants Nos. 17310084, 17760082, and 17656044, 2005, and Handai Frontier Research Center. Work of one of the authors (S.O.) is supported by the Next Generation Supercomputer Project, Nanoscience Program, MEXT, Japan. Work of one of the authors (J.L.) is supported by NSF Grant No. DMR-0502711, AFOSR Grant No. FA9550-05-1-0026, ONR Grant No. N00014-05-1-0504, National Energy Technology Laboratory Grant No. DE-AM26-04NT41817, and Ohio Supercomputer Center.

*Electronic address: nakayama@pe.osakafu-u.ac.jp

[1] Y. Nakayama, A. Nagataki, O. Suekane, X. Cai, and S. Akita, Jpn. J. Appl. Phys., Part 2 **44**, L720 (2005).
[2] A. J. Stone and D. J. Wales, Chem. Phys. Lett. **128**, 501 (1986).
[3] B. I. Yakobson, Appl. Phys. Lett. **72**, 918 (1998).
[4] Q. Zhao, M. B. Nardelli, and J. Bernholc, Phys. Rev. B **65**, 144105 (2002).
[5] P. Zhang, P. E. Lammert, and V. H. Crespi, Phys. Rev. Lett. **81**, 5346 (1998).
[6] M. B. Nardelli, B. I. Yakobson, and J. Bernholc, Phys. Rev. Lett. **81**, 4656 (1998).
[7] P. Jensen, J. Gale, and X. Blase, Phys. Rev. B **66**, 193403 (2002).
[8] Z. Li, P. Dharap, P. Sharma, S. Nagarajaiah, and B. I. Yakobson, J. Appl. Phys. **97**, 074303 (2005).
[9] G. G. Samsonidze, G. G. Samsonidze, and B. I. Yakobson, Phys. Rev. Lett. **88**, 065501 (2002).
[10] T. Dumitrica and B. I. Yakobson, Appl. Phys. Lett. **84**, 2775 (2004).
[11] S. Berber, Y.-K. Kwon, and D. Tomanek, Phys. Rev. Lett. **91**, 165503 (2003).
[12] T. Belytschko, S. P. Xiao, G. C. Schatz, and R. Ruoff, Phys. Rev. B **65**, 235430 (2002).
[13] J. Y. Huang, S. Chen, Z. Q. Wang, K. Kempa, Y. M. Wang, S. H. Jo, G. Chen, M. S. Dresselhaus, and Z. F. Ren, Nature (London) **439**, 281 (2006).
[14] D. Tekleab, D. L. Carroll, G. G. Samsonidze, and B. I. Yakobson, Phys. Rev. B **64**, 035419 (2001).
[15] D. Bozovic, M. Bockrath, J. H. Hafner, C. M. Leiber, H. Park, and M. Tinkham, Phys. Rev. B **67**, 033407 (2003).
[16] T. Kuzumaki, S. Kitakata, K. Enomoto, T. Yasuhara, N. Ohtake, and Y. Mitsuda, Carbon **42**, 2343 (2004).
[17] A. Hashimoto, K. Suenaga, A. Gloter, K. Urita, and S. Iijima, Nature (London) **430**, 870 (2004).
[18] F. C. Frank and W. T. Read, Phys. Rev. **79**, 722 (1950).
[19] B. I. Dunlap, Phys. Rev. B **46**, 1933 (1992).
[20] L. Chico, V. H. Crespi, L. X. Benedict, S. G. Louie, and M. L. Cohen, Phys. Rev. Lett. **76**, 971 (1996).
[21] J. Han, M. P. Anantram, R. L. Jaffe, J. Kong, and H. Dai, Phys. Rev. B **57**, 14983 (1998).
[22] T. Zhu, J. Li, and S. Yip, Phys. Rev. Lett. **93**, 025503 (2004).
[23] T. Zhu, J. Li, and S. Yip, Phys. Rev. Lett. **93**, 205504 (2004).
[24] I. I. Oleinik and D. G. Pettifor, Phys. Rev. B **59**, 8500 (1999).
[25] G. Henkelman and H. Jonsson, J. Chem. Phys. **113**, 9978 (2000).
[26] D. G. Pettifor and I. I. Oleinik, Phys. Rev. B **59**, 8487 (1999).
[27] D. G. Pettifor and I. I. Oleinik, Phys. Rev. Lett. **84**, 4124 (2000).
[28] J. Li, K. J. Van Vliet, T. Zhu, S. Yip, and S. Suresh, Nature (London) **418**, 307 (2002).
[29] X. Cai, S. Akita, and Y. Nakayama, Thin Solid Films **464-465**, 364 (2004).
[30] J. Li, C. Z. Wang, J. P. Chang, W. Cai, V. V. Bulatov, K. M. Ho, and S. Yip, Phys. Rev. B **70**, 104113 (2004).